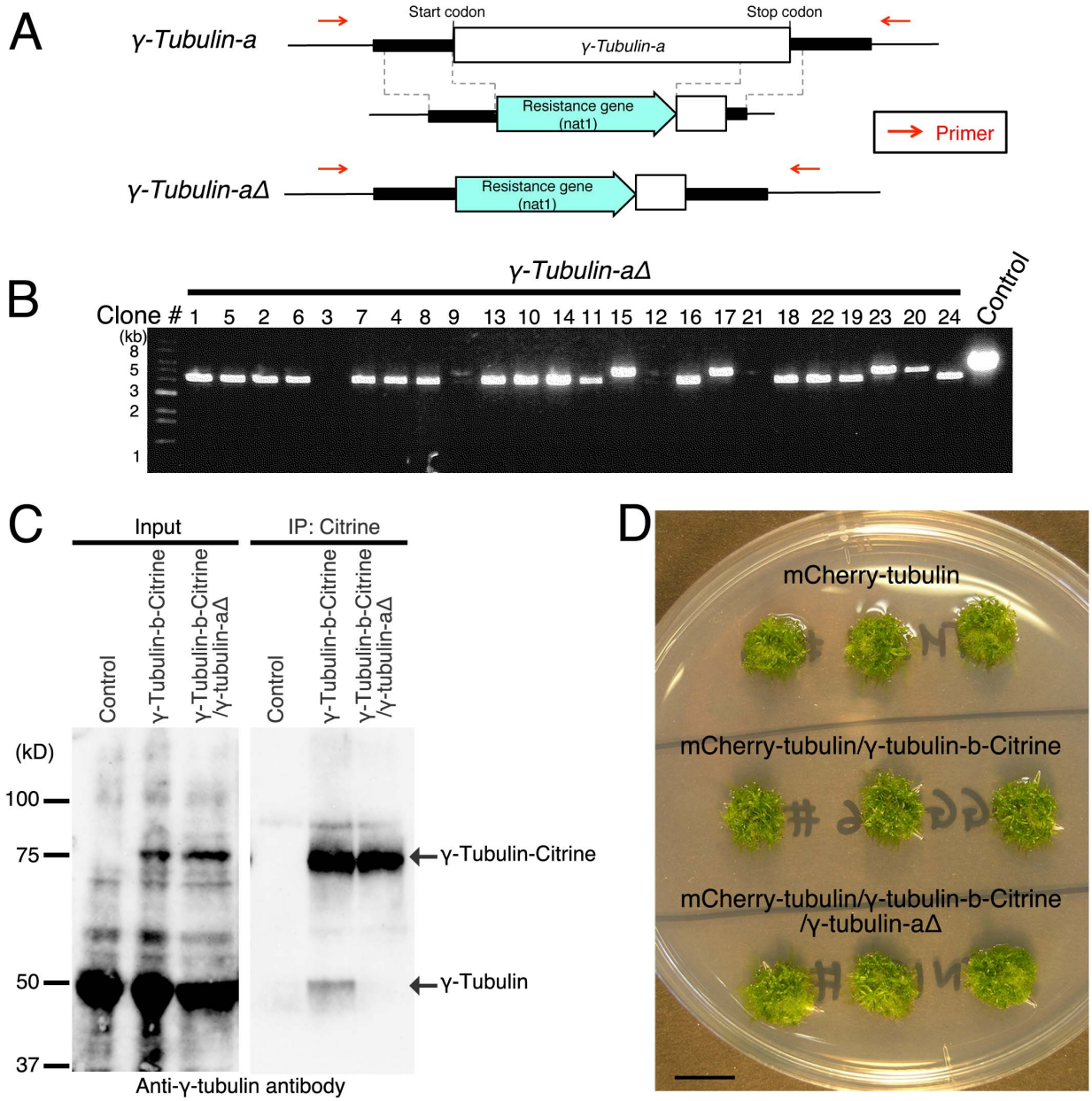

Figure S1. Construction of the γ-tubulin-Citrine replacement line

(**A**) *P. patens* has two paralogous γ-tubulin genes, *γ-tubulin-a* and *γ-tubulin-b*, both of which are expressed in protonemal cells (Nakaoka et al., 2012). By using homologous recombination, we deleted the *γ-tubulin-a* (*TubG1*) gene, while endogenous *γ-tubulin-b* (*TubG2*) was tagged with *citrine* (the latter was done in (Nakaoka et al., 2012)). The established moss line thus expresses Citrine-tagged γ-tubulin but not untagged γ-tubulin. Red arrows indicate PCR primers used to verify homologous recombination. (**B**) Confirmation of the *γ-tubulin-a* deletion by PCR. A 4.3-kb band appeared when homologous recombination occurred (5.0 kb in the control line). (**C**) Confirmation of the *γ-tubulin-a* deletion by immunoblotting. We immunoprecipitated γ-tubulin-b-Citrine with the anti-GFP antibody, following which we performed immunoblotting using the G9 antibody that recognises two paralogous *P. patens* γ-tubulin proteins (Horio et al., 1999; Nakaoka et al., 2012). In control cells that express both γ-tubulin-b-Citrine and untagged γ-tubulin-a, a 50-kD band was detected, which corresponds to untagged γ-tubulin-a. The interaction between γ-tubulin-b-Citrine and γ-tubulin-a was expected, since a γ-tubulin ring complex should contain ~13 γ-tubulin subunits (Choi et al., 2010; Kollman et al., 2010). In contrast, for the γ-tubulin-b-Citrine/γ-tubulin-a-delta line that was used in this study, the 50-kD band was undetectable, indicating that untagged γ-tubulin is absent in this line. We added the immunoprecipitation step prior to immunoblotting because the G9 antibody cross-reacted with a protein having molecular weight similar to that of γ-tubulin (~50 kD) when the whole-cell extract was directly immunoblotted. We concluded that our γ-tubulin-b-Citrine line indeed expresses only tagged γ-tubulin. (**D**) The γ-tubulin-b-Citrine replacement line (mCherry-tubulin is also expressed) grew and developed normally in our culture conditions. The images were acquired ~3 weeks after inoculation of a piece of protonemata onto the BCDAT agar medium. Bar, 10 mm.

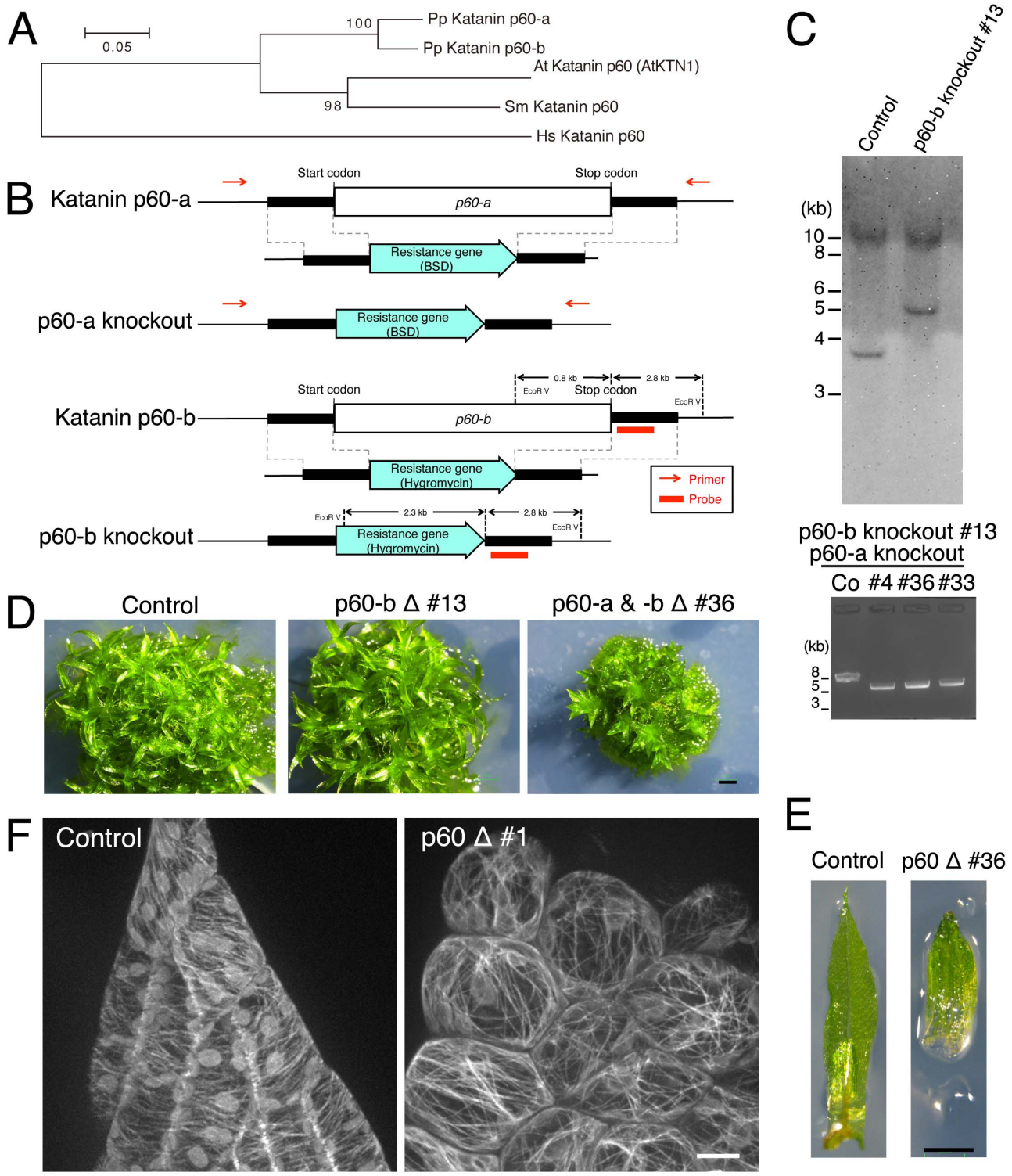

Figure S2. Construction of the katanin p60 disruptant

(**A**) Phylogenetic tree of katanin p60 proteins of *Physcomitrella patens* (Pp), *Arabidopsis thaliana* (At), *Selaginella moellendorffii* (Sm), and *Homo sapiens* (Hs). The procedure of (Miki et al., 2014) was followed for construction. In brief, the numbers on the branches represent the local bootstrap probability. The local bootstrap values with 1,000 replicates are shown on branches. The horizontal branch length is proportional to the estimated evolutionary distance. The bar indicates the number of amino acid substitutions per site. *P. patens* has two highly similar katanin p60 subunit proteins (named katanin p60-a and -b). (**B**) Scheme of gene disruption of two katanin p60 genes. Homologous recombination was expected to occur at the 5' and 3'UTRs (black bars). Red bars indicate the Southern hybridisation probes, whereas red arrows indicate PCR primers. (**C**) (Top) Southern hybridisation confirmed *p60-b* knockout. Control is the parental GFP-tubulin line (Bottom) PCR confirmed *p60-a* deletion in the background of *p60-b* disruptant (#4, #33, and #36 clones). Co stands for control. (**D**) Gametophores did not display good development in the p60 disruptant. Bar, 1 mm. (**E**) Leaves were shorter in the katanin p60 disruptant than in the control line. Bar, 0.5 mm. (**F**) Cortical MTs labelled with GFP-tubulin in the gametophore leaf cells. Images were acquired with spinning-disc confocal microscopy, and maximum projection images of 36 z-stacks (0.5 µm intervals) are displayed. Transversely oriented cortical MT arrays were observed in the control cells, whereas the MTs were disorganised and individual cells were swollen in the disruptant. Note that chloroplasts are also visualised in these images due to autofluorescence. Bar, 10 µm.

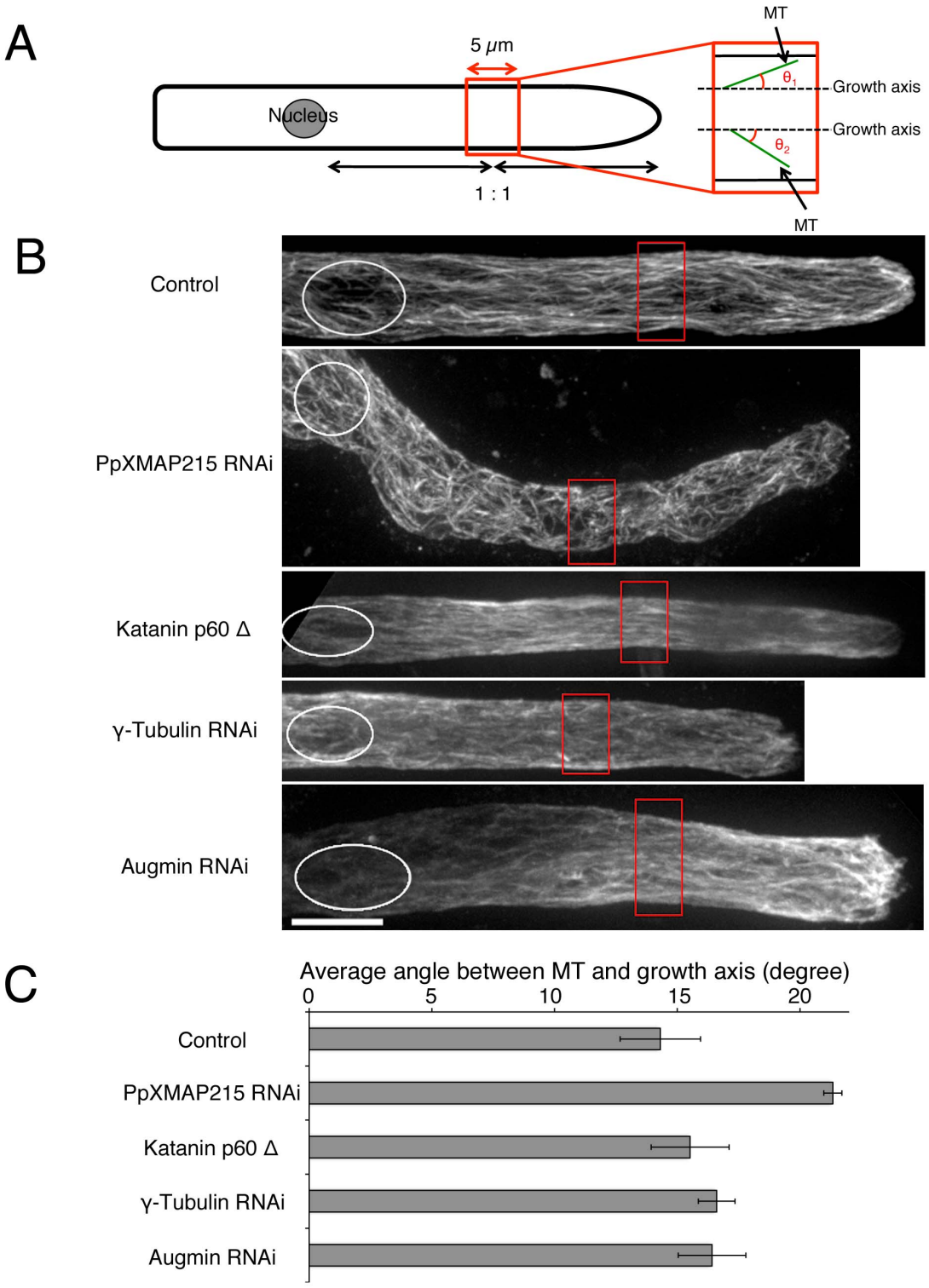

Figure S3. Orientation of endoplasmic MTs is not significantly changed in γ-tubulin RNAi- or augmin (Aug3) RNAi-treated cells

(**A**) The angle θ (0–90°) was measured to assess the orientation of the individual MTs. (**B**) Representative immunofluorescence images of MTs in the protonemal apical cell. Maximum projection images of 27 z-stacks (each separated by 0.5 μm) are shown. Nuclear position (white) and the analysed region (red) are marked. Many apical cells were bent after PpXMAP215 RNAi treatment, while the majority of cells receiving the other RNAi treatments had a straight shape. We, therefore, analysed the bent cells for PpXMAP215 and the straight ones for the other proteins. Bar, 10 μm. (**C**) Overall MT polarity in each RNAi-treated sample. Approximately 60 MTs from 3–6 cells were analysed. MTs were identified in every three frames of z-stacks for three to four frames. The mean value of θ was obtained for each cell, and the values were averaged. Other than PpXMAP215 ($p = 0.022$), depletion did not significantly affect the polarity (± SEM, $p > 0.2$).

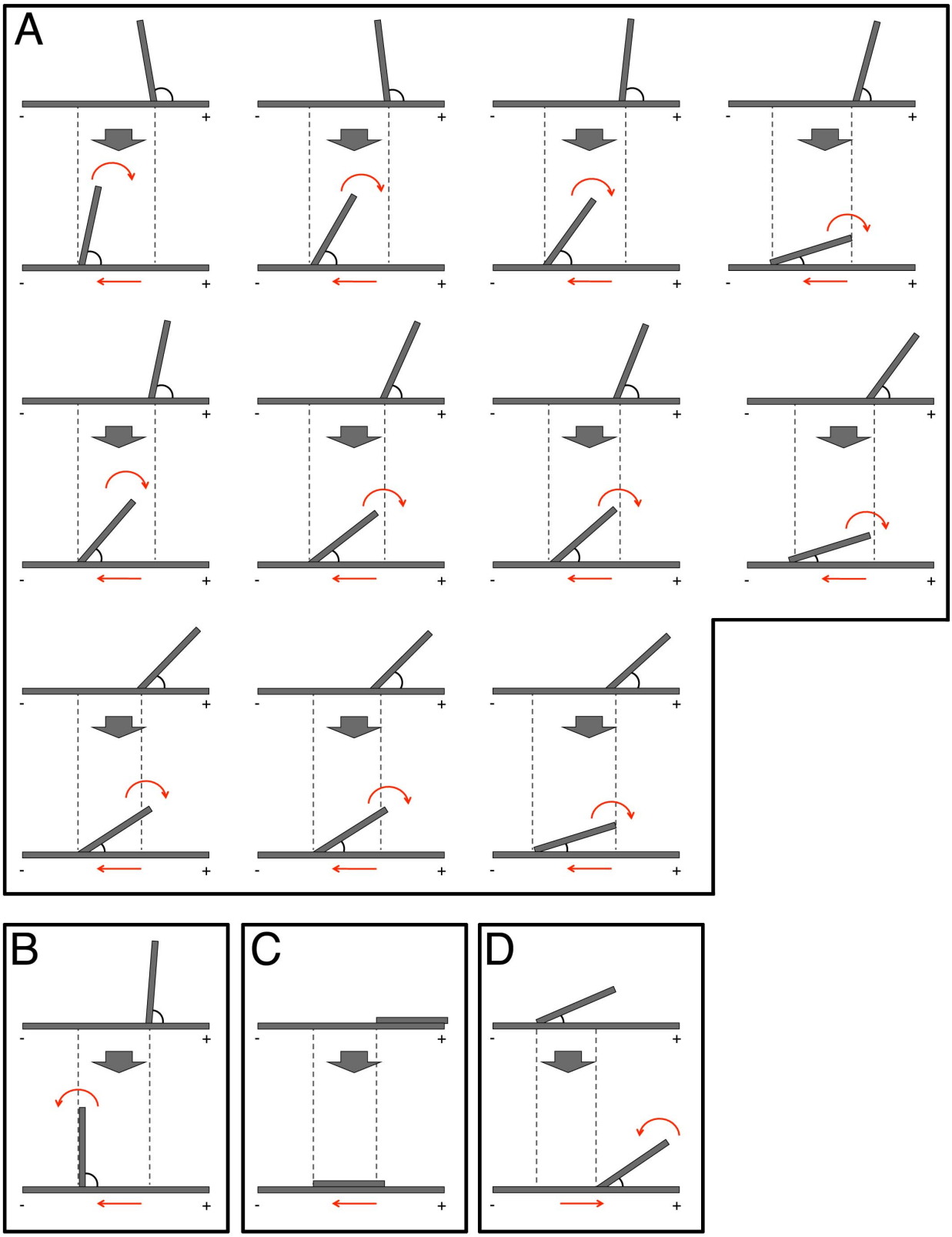

Figure S4. Summary of daughter MT migration after branching nucleation

We encountered 14 cases in which the daughter MTs migrated along the mother MTs, the polarities of which could be determined. (**A–C**) In 13 of them, the migration was towards the minus-end of mother MTs (straight red arrows indicate the directionality). Eleven of those 13 migrating MTs had shallower branch angles relative to the mother MTs after migration (**A**) (curved red arrows indicate the angle change). The branch angle was wider after migration in one case (**B**), whereas the angle was unchanged in another case (**C**, parallel nucleation). Thus, minus-end-directed transport of daughter MTs might be a means to orient two MTs in a uniform polarity. (**D**) Plus-end-directed migration was observed for only one case.

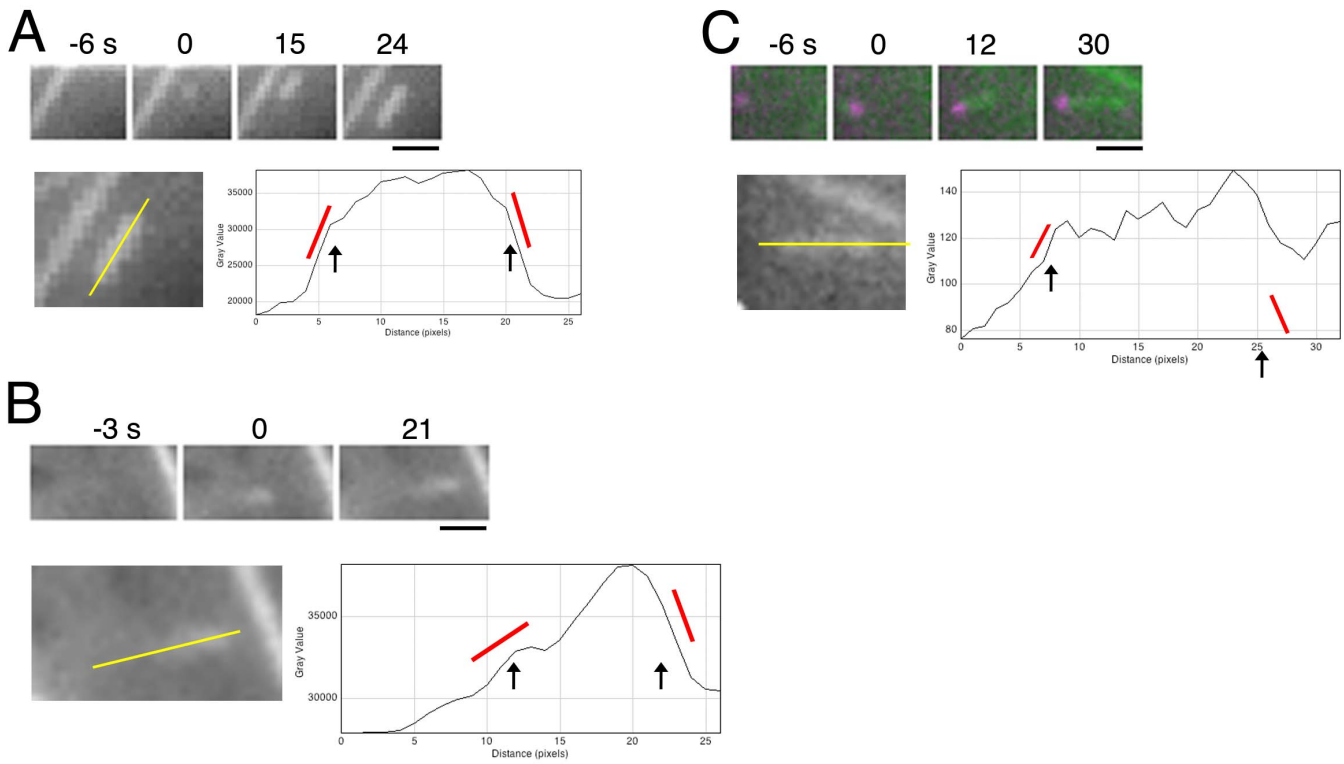

Figure S5. Criteria for identification of cytoplasmic nucleation

(**A**) (Top) An example of cytoplasmic nucleation visualised by GFP-tubulin. (Bottom) Profile of signal intensity along the short MT displayed in the top panel (24 s). The Citrine signal declines steeply at both ends of the MT (arrows and red bars). (**B**) (Top) An example of the appearance of the growing MT plus-end (GFP-tubulin). (Bottom) The profile of signal intensity along the MT displayed in the top panel (21 s) indicates that the GFP signal decreases gently at the left end of the MT (arrow and red bar). (**C**) (Top) An example of cytoplasmic nucleation. One end of the MT (green; mCherry-tubulin) was capped by γ-tubulin (magenta; γ-tubulin-b-Citrine). Note that the MT showed a pivot turn during time 0–12 s. (Bottom) Profile of signal intensity along the short MT displayed in the top panel (30 s). The mCherry signal declines steeply at both ends of the MT (arrows and red bars). Bars, 1 μm.

When interpreting the origin of a GFP-tubulin spot, we considered the caveat that an observed spot might represent a growing MT end rather than the nucleation point (e.g. where a MT nucleated outside the focal plane grew and entered into the focal plane). We identified true nucleation events using the following criteria. First, when a small spot showed diffusible motion, we concluded that it was a bona fide MT nucleation point, because such motion would not be observed at the MT plus end (**A**). Second, when diffusible motion was not detected, but where the GFP signal declined steeply at both ends of the MT, we concluded that the emerging short MT was newly nucleated (**A**). However, where GFP intensity decreased gradually at only one end of the short MT, we classified the object as a MT plus end that had grown from the off-focal plane (**B**). Consistent with these criteria, in most cases we found γ-tubulin at the end of short MTs in which the mCherry signal declined steeply at both ends, but not where it declined gradually at one end (**C**). Another caveat was that new MTs that are generated out of the 2-D focal plane could be re-directed into the focal plane by diffusion; this might skew the quantification of the event number compared to the branching nucleation in which the daughter MTs could be less diffusive. However, the reverse is also true; cytoplasmically nucleated MTs in the observed focal plane sometimes diffused to other focal planes. Therefore, we consistently counted only the nucleation event that occurred in the observed focal plane.

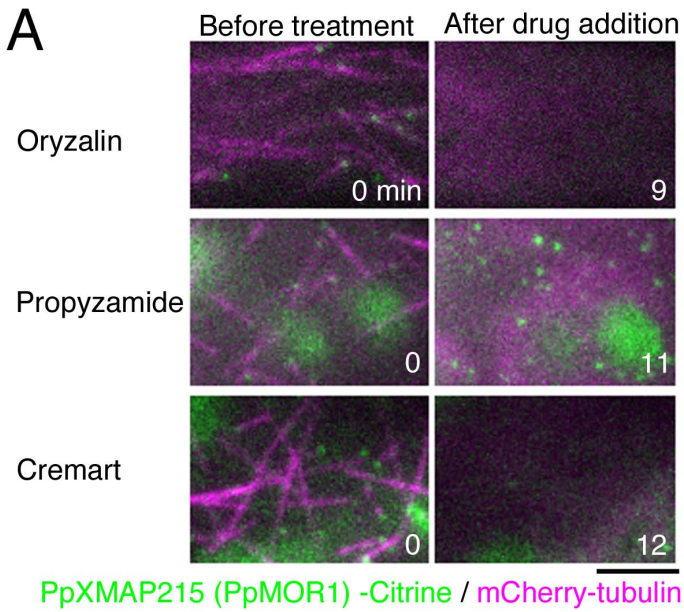

Figure S6. Effectiveness of 3 MT destabilisation drugs

(**A**) Cells expressing PpXMAP215/PpMOR1-a-Citrine (green) and mCherry-tubulin (magenta) were treated with 40 μM oryzalin, 200 μM propyzamide, or 50 or 100 μM cremart for 12 min. PpXMAP215-a-Citrine was accumulated at the tip of MTs in untreated cells. MT signals disappeared after each drug treatment. However, PpXMAP215-a-Citrine was clearly visible after propyzamide treatment, suggesting that undetectable levels of MTs were resistant to the drug treatment. PpXMAP215-a-Citrine was also detected in the case of cremart, albeit more sparsely. Note that large green signals represent autofluorescent chloroplasts. (**B**) MT regrowth after washing out oryzalin, propyzamide, or cremart. In each case PpXMAP215-a-Citrine was found at the tip of MTs. Note that giant green signals represent autofluorescent chloroplasts. Bars, 5 μm.

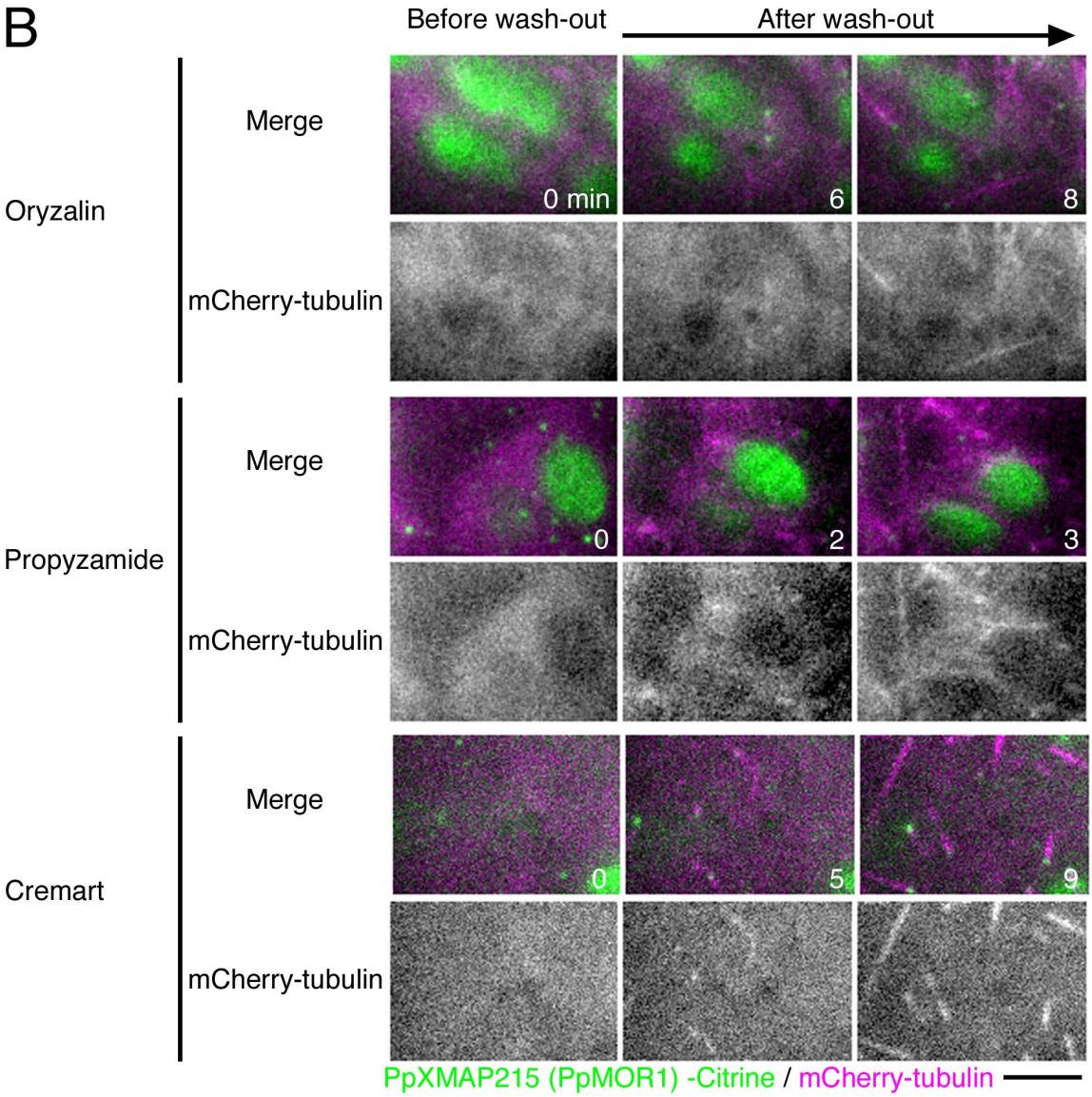

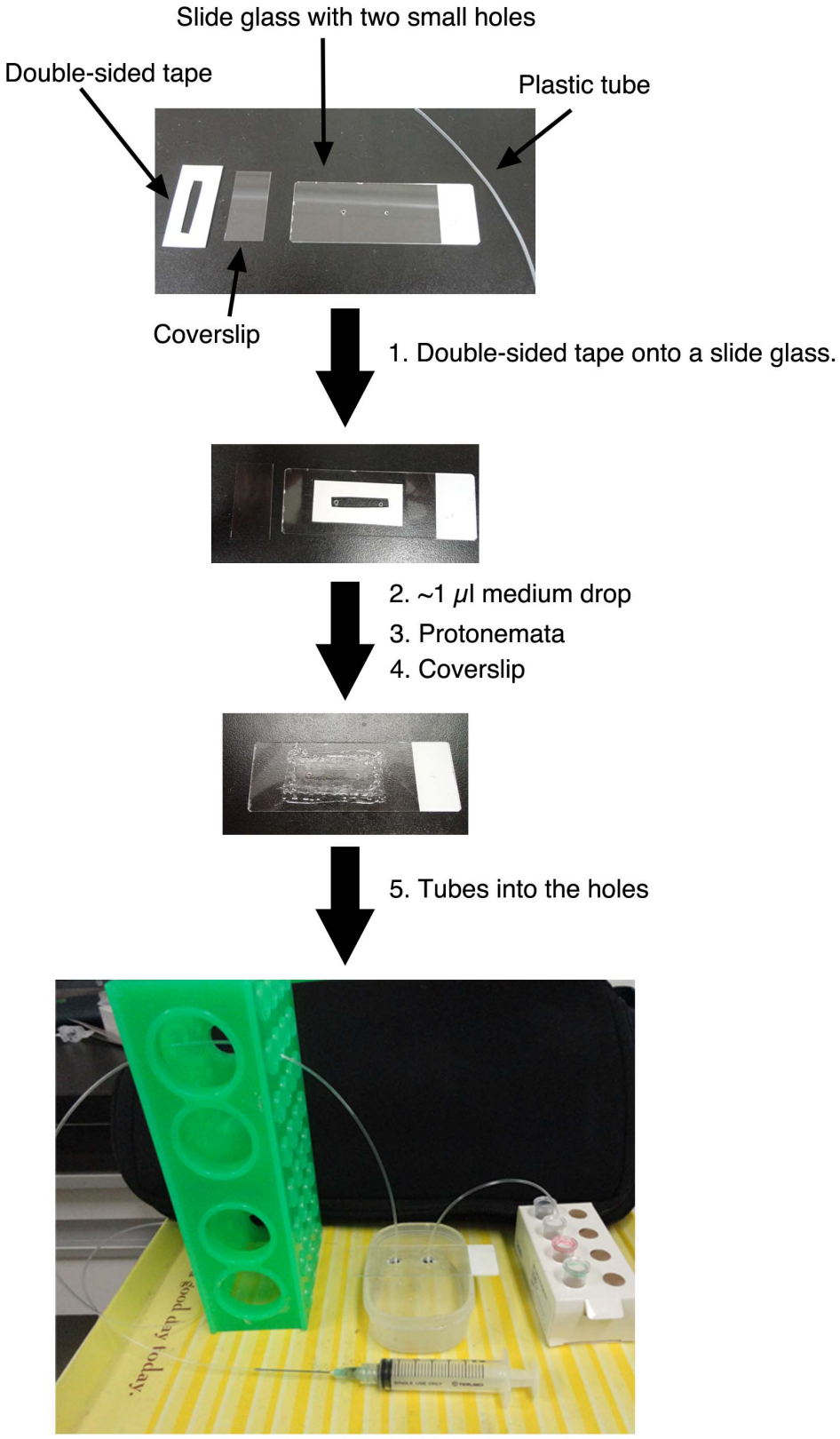

Figure S7. MT depolymerisation-regrowth assay using a syringe pump

We prepared plastic tubes, double-sided tape, a coverslip, and a slide glass in which two holes were made. Protonemal cells were placed between the two holes, and sealed with the coverslip and the double-sided tape. The medium was supplied or exchanged at 50 µL/min flow rate through two plastic tubes that were associated with 2 mL tube and a 5-mL plastic syringe. Harvard Apparatus Pump 11 Elite was used as the syringe pump.

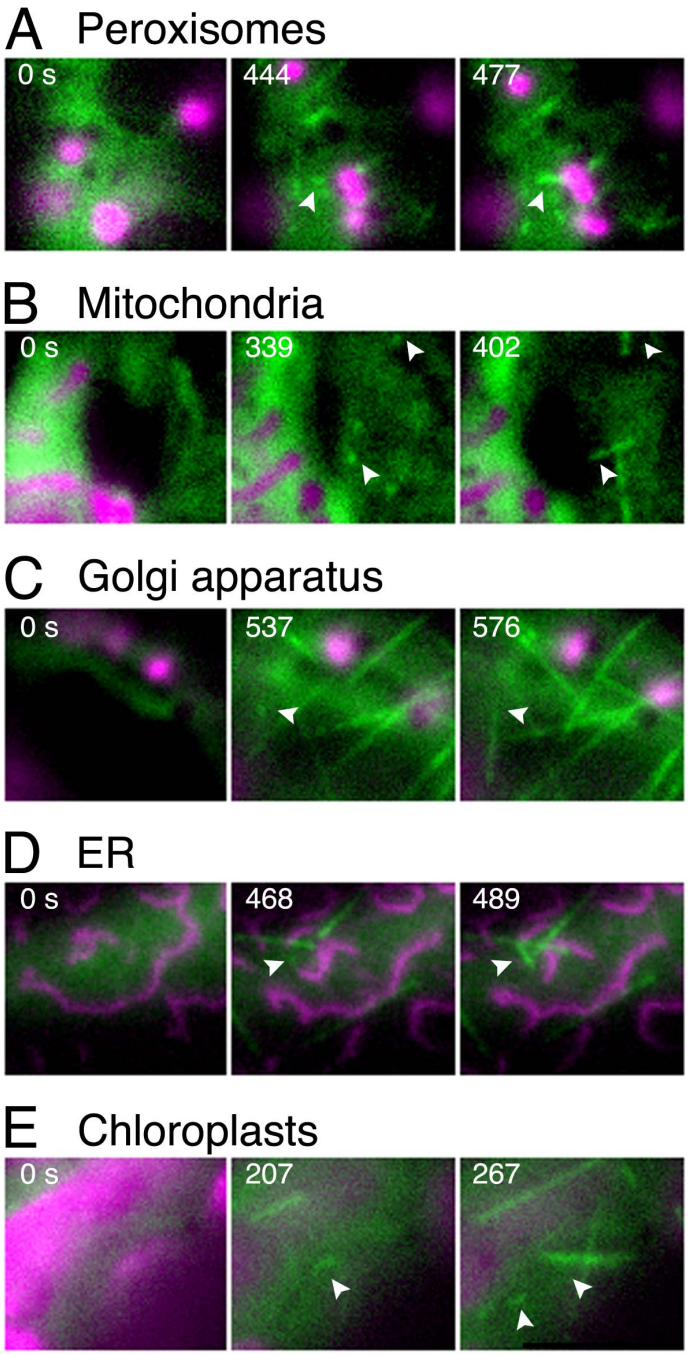

Figure S8. Cytoplasmic nucleation does not occur at a specific organelle

MT regrowth assay was performed in cells expressing markers of the peroxisome (**A**), mitochondrion (**B**), Golgi apparatus (**C**), and endoplasmic reticulum (ER) (**D**). MTs were labelled with GFP-tubulin (green), whereas organelle markers were constructed with mCherry or RFP tagging (magenta). Chloroplasts were visualised by 640 nm laser illumination (**E**). Arrowheads indicate cytoplasmic nucleation that did not occur at the marked organelle. See also Movie 7. Bar, 5 μm.

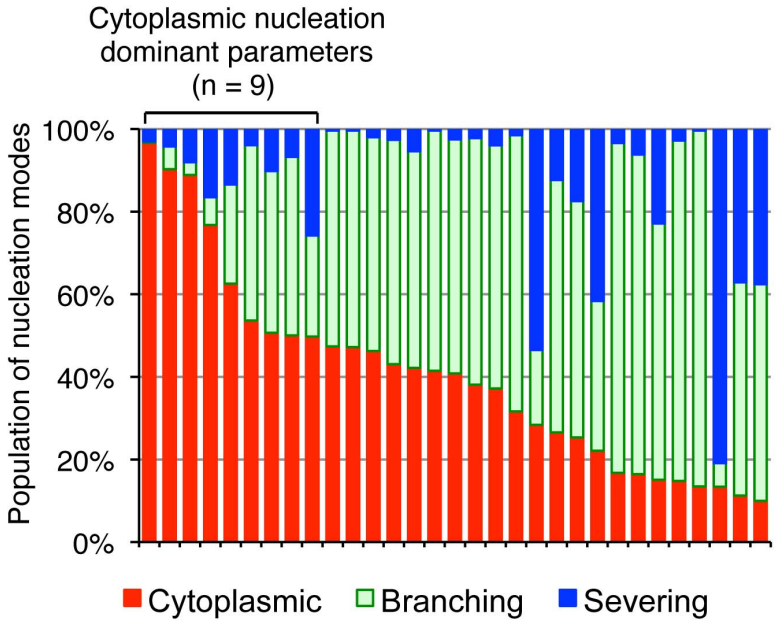

Figure S9. Supplementary data for numerical modelling

The three modes of nucleation observed in the simulation from 0–7 min after the onset of regrowth. Each bar represents a set of parameters obtained from an individual fitting trial (n = 31). The parameter sets that reproduce dominance in cytoplasmic nucleation are indicated (n = 9). Red: cytoplasmic nucleation, green: branching nucleation, and blue: severing.

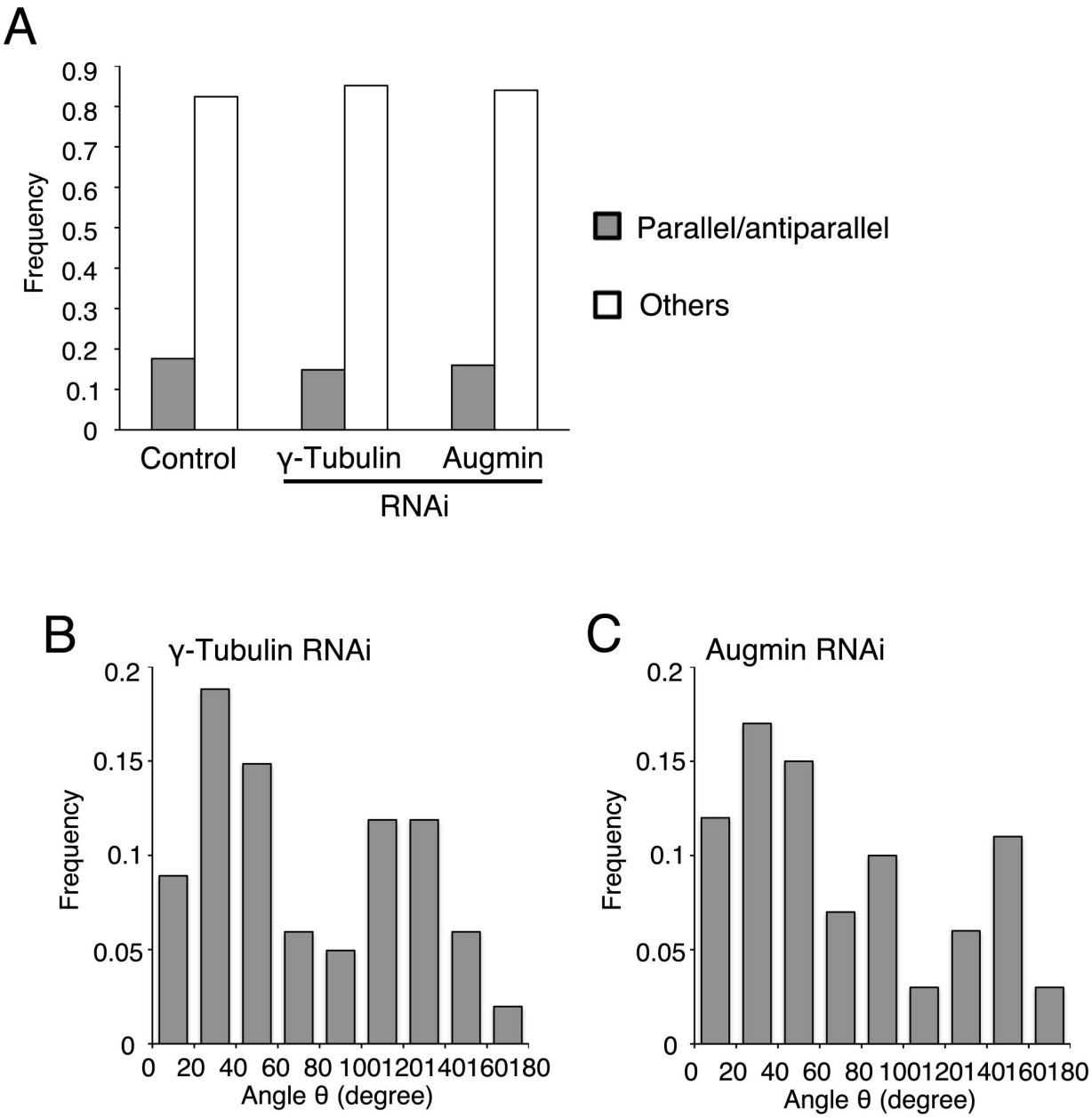

Figure S10. Branch angle is unchanged after γ-tubulin or augmin RNAi treatment

(**A**) Branching nucleation was subdivided into two categories: parallel/antiparallel nucleation and nucleation with a branch angle between 0° and 180°. γ-Tubulin or augmin (Aug3) RNAi did not affect the ratio of these two modes. The control cell data are the duplicate of those presented in Fig. 2C. (**B**) Angles between mother and daughter MTs in cells knocked down for γ-tubulin (n = 86) or augmin (n = 84). Parallel/antiparallel nucleation was excluded from the analysis. The angle was measured at 9–15 s after daughter MT appearance. A wide range of angles was observed, including those above 90°. No significant difference was observed between these and the control data (compare with Fig. 2D).

Table S1. Eleven unfixed parameters used for modelling

Symbol		Search range
Tubulin concentration		
TubTot	Number of total tubulin monomers per unit area* (1 unit = 0.25 μm of MT)	3,000-10,000
Simulation specific parameter		
NucTot	Number of potential nucleation sites per area	200-400
Cytoplasmic nucleation		
NucRate	Rate of cytoplasmic nucleation [/s area] is defined as ***NucTot*** × ***NucRate*** × (***FreeTub***/***TubTot***)^{NucAlpha}. ***FreeTub*** [unit] = ***TubTot*** [unit] – total length of MTs [unit].	0 - 1
NucAlpha		0 - 10
Branching nucleation		
MDMNRate	Rate of branching (MT-dependent MT) nucleation [/s μm of MT] is defined as ***MDMNRate*** × (***FreeTub***/***TubTot***)^{MDMNAlpha} × 4.	0 - 0.1
MDMNAlpha		0 - 10
Severing		
SevRate	Rate of severing [/s μm of MT] is defined as ***SevRate*** × 4.	0 - 0.1
Dynamic instability of MTs		
FreqCat	Catastrophe frequency of MTs [/s]	0 - 1
FreqRes	Rescue frequency of MTs [/s]	0 - 1
Kgrowth	Growth velocity of MTs [μm/s] is defined as ***Kgrowth*** × (***FreeTub***/***TubTot***) × 0.25.	0 - 2
Kshrink	Shrinkage velocity of MTs [μm/s] is defined as ***Kshrink*** × 0.25.	0 - 2

* Unit area in the simulation was 1,120 μm^2

Table S2. The number and length of MTs observed in the MT regrowth assay used for fitting with the numerical model

	Time after wash-out [min]	Value [$\times 10^{-2}$]
Number of total MTs [/μm^2]	3	1.5
	4	3.1
	5	5.9
	6	7.1
	8	7.7
	10	8.7
	12	8.4
Number of growing MTs [/μm^2]	3	1.5
	5	4.7
	12	6.0
Number of shrinking MTs [/μm^2]	5	1.3
	12	2.5
Total length of MTs [μm/μm^2]	4	8.2
	6	22
	12	47

Table S3. List of transgenic lines used in this study

Gene	Clone #	Background	Source
PpXMAP215/PpMOR1 RNAi	#7	GFP-tubulin /H2B-mRFP	(Nakaoka et al., 2012)
γ-Tubulin RNAi	#12		(Nakaoka et al., 2012)
Aug3 RNAi	#12		(Nakaoka et al., 2012)
Katanin p60 deletion	#36	GFP-tubulin (rice actin promoter)	This study
Katanin p60 deletion	#1, 2	GFP-tubulin (EF1α promoter)	This study
γ-Tubulin-b (TubG2) -Citrine / *γ-tubulin-a (TubG1)Δ*	#1	mCherry-tubulin	This study
PpXMAP215/PpMOR1-a-Citrine	#7		This study
Mitochondrion-mRFP (tagged to γATPase)	#1	GFP-tubulin	(Uchida et al., 2011)
ER-mCherry	#21		Gift from Shu-Zon Wu and Magdalena Bezanilla
Golgi-mRFP (tagged to *P. patens* Man1's N-terminus)	#3		Constructed in this study, referring to (Furt et al., 2012)
Peroxisome-mCherry (mCherry-SKL expression)	#2		This study

Table S4. List of PCR primers used in this study

Gene	5' primer	3' primer
PpXMAP215 /PpMOR1 -a-Citrine	AAAggtaccCCTCAGGTGCGAAG CTTGTGC	AAAatcgatATACTCTGAACCCC CGCCAGC
	AAAggatccCCACCTGAAGACGA TAATCATTTGC	AAAtctagaAGCCCTGGAACGT CCTAGGGACTG
(for integration check)	GCTGCAGTGTTCAAGAAGATC GGTG	GCAGAGCAGGAGCCCATCAG CGAG
γ-Tubulin-a knockout	AAActcgagCCAACCACCAAGTG AGTGAGACTTC	AAAgatatcCTTGGTCGCGCTTT CTTCAGACC
	AAAggatccCAATGCGAATGGAG GTTGCAGG	AAAccgcggCGTGCTCAGACCA GATGTGTG
(for integration check)	CAGCCTTGACATGTGGAGATA GTTG	ATGCTTGGCAGCAGTGGAGA AGCTC
PpMan1-RFP	ATAgcggccgcCCCCTTCACCAT GGCAATTCAGAGTCGAAGATC	TATggcgcgccCACCCTTATTAT GGCGATCCCATAGGAAG
Peroxisome-mCherry	ATAgcggccgcCCCCTTCACCAT GGTTTCTAAAGGAGAAGAAGA CAATATG	TATggcgcgccCACCCTTTTACA ACTTAGATTTATACAATTCAT CCATTCCTCCAG
Katanin p60-a knockout	GGggtaccGATTCTCACTCACGC CATCACG	CCGctcgagACTGTTCTCGTCC CGCAATCAC
	CGggatccGCTTCTGATGTAAAC GATGGAGC	TCCccgcggACTTCGCATGTGA GAGCCACC
(for integration check)	CATCGAGTTCTTGTCCTTGACA CATACTC	GAGGTTGATATCTAAGAGAT GATCAAAGCAC
Katanin p60-b knockout	GGggtaccGCCATTCAAGCCATT CGAGAATGG	CCGctcgagGCTGTCCTCCTCG TCCCGCAAC
	CGggatccGATCAGGATGTAAAT GATGCATCTGG	TCCccgcggGCACATGAACTTA CATAAGTGGTGC

Restriction enzyme sites are marked with lower cases

References

Choi, Y.K., Liu, P., Sze, S.K., Dai, C., and Qi, R.Z. (2010). CDK5RAP2 stimulates microtubule nucleation by the gamma-tubulin ring complex. J Cell Biol **191,** 1089-1095.

Furt, F., Lemoi, K., Tuzel, E., and Vidali, L. (2012). Quantitative analysis of organelle distribution and dynamics in Physcomitrella patens protonemal cells. BMC Plant Biol **12,** 70.

Horio, T., Basaki, A., Takeoka, A., and Yamato, M. (1999). Lethal level overexpression of gamma-tubulin in fission yeast causes mitotic arrest. Cell Motil Cytoskeleton **44,** 284-295.

Kollman, J.M., Polka, J.K., Zelter, A., Davis, T.N., and Agard, D.A. (2010). Microtubule nucleating gamma-TuSC assembles structures with 13-fold microtubule-like symmetry. Nature **466,** 879-882.

Miki, T., Naito, H., Nishina, M., and Goshima, G. (2014). Endogenous localizome identifies 43 mitotic kinesins in a plant cell. Proc Natl Acad Sci U S A **111,** E1053-1061.

Nakaoka, Y., Miki, T., Fujioka, R., Uehara, R., Tomioka, A., Obuse, C., Kubo, M., Hiwatashi, Y., and Goshima, G. (2012). An inducible RNA interference system in Physcomitrella patens reveals a dominant role of augmin in phragmoplast microtubule generation. Plant Cell **24,** 1478-1493.

Uchida, M., Ohtani, S., Ichinose, M., Sugita, C., and Sugita, M. (2011). The PPR-DYW proteins are required for RNA editing of rps14, cox1 and nad5 transcripts in Physcomitrella patens mitochondria. FEBS Lett **585,** 2367-2371.